Dalton Transactions

ROYAL SOCIETY OF CHEMISTRY

PAPER

View Article Online
View Journal | View Issue

Cite this: *Dalton Trans.*, 2025, **54**, 1150

In situ growth of octa-phenyl polyhedral oligomeric silsesquioxane nanocages over fluorinated graphene nanosheets: super-wetting coatings for oil and organic sorption†

Pushparaj Loganathan,[a,c] Ravi Yogapriya,[b] Arunkumar Chinnusamy,[a] K. K. R. Datta *[b] and Swaminathan Shanmugan *[a]

Superhydrophobic surfaces offer significant advantages through their hierarchical micro/nanostructures, which create optimal surface roughness and low surface energy, making the development of robust surfaces essential for enhancing their physical and chemical stability. Here, we introduce *in situ* growth of octa-phenyl polyhedral oligomeric silsesquioxane (O-Ph-POSS) nanocages over multi-layered fluorinated graphene (FG) nanosheets through hydrolysis/condensation of phenyl triethoxysilane in an alkaline medium to produce a robust POSS–FG superhydrophobic hybrid. The efficient *in situ* growth of O-Ph-POSS nanocages over FG nanosheets was confirmed by FT-IR spectroscopy, PXRD, SEM, TEM, TG analysis, ^{29}Si NMR spectroscopy, N_2 adsorption–desorption isotherms and XP spectroscopy. The as-synthesized O-Ph-POSS over FG becomes superhydrophobic with a water contact angle (WCA) of 152 ± 2° and a surface free energy (SFE) of 5.6 mJ m^{-2}. As a result of the superhydrophobic property and robust nature of the POSS nanocage, O-Ph-POSS over FG nanosheets revealed the absorption capability for oils/organic solvents ranging from 200 to 500 wt% and were applied to coat onto the polyurethane (PU) sponge to effectively separate various oils and organic solvents from water mixtures, achieving separation efficiencies between 90% and 99%. Importantly, O-Ph-POSS-FG@Sponge still retained a separation efficiency of over 95% even after 25 separation cycles for hexane spill in water. The sponge efficiently separates toluene and chloroform using a vacuum pump, achieving flux rates of up to 20 880 and 12 184 L m^{-2} h^{-1}, respectively. Weather resistance tests of O-Ph-POSS-FG@Sponge, prepared at intervals of 1 week and 1 year, showed that aged samples retained similar WCA values to freshly prepared sponges, confirming their long-term durability and performance. Mechanical stability assessments indicated that O-Ph-POSS-FG@Sponge maintained superhydrophobic properties, with WCA values of 151 ± 2° for tape peeling and emery paper treatments and 150 ± 2° for knife cutting, highlighting its excellent stability under physical deformation. Additionally, leveraging the exceptional resistance of O-Ph-POSS, the superhydrophobic O-Ph-POSS-FG@Sponge exhibited excellent stability and durability, even under supercooled and hot conditions during oil/water separation. Optical microscopy analysis of O/W and W/O emulsions, both stabilized by a surfactant, revealed complete droplet separation, further confirming the O-Ph-POSS-FG@Sponge's effectiveness for emulsion separation applications. The present work provides a straightforward method for the large-scale production of robust, superhydrophobic materials suitable for cleaning up oil spills on water surfaces.

Received 20th September 2024,
Accepted 19th November 2024

DOI: 10.1039/d4dt02678k

rsc.li/dalton

Introduction

Recently, oil and organic solvent spills occurring in oceans and rivers have damaged the marine systems largely, impacting both ecology and the aquatic environment.[1–4] To address this burgeoning issue, many conventional and traditional techniques such as booming, skimming, absorption, *in situ* burning, dispersants, and bioremediation, have been used to treat oil/organic spills from marine bodies and oil

[a]*Department of Chemistry, Faculty of Engineering and Technology, SRM Institute of Science and Technology, Kattankulathur-603203, Tamil Nadu, India. E-mail: shanmugs2@srmist.edu.in, shanmugan0408@gmail.com*
[b]*Functional Nanomaterials Laboratory, Department of Chemistry, Faculty of Engineering and Technology, SRM Institute of Science and Technology, Kattankulathur-603203, Tamil Nadu, India. E-mail: kumarard@srmist.edu.in, kkrdatta@gmail.com*
[c]*Department of Chemistry, Christ University, Bengaluru, Karnataka 560029, India*
† Electronic supplementary information (ESI) available. See DOI: https://doi.org/10.1039/d4dt02678k

industries.[5–7] Absorption is a highly practical technique, widely favored for its ability to enable complete recovery of spilled oil and its ease of assembly. Several absorbent materials such as zeolites, organoclays, activated carbons and modified cotton fibers have been used; however, they exhibit poor separation efficiency where absorption of both oil and water can occur simultaneously.[8–13] This demands the development of extremely liquid-repellent surfaces by mimicking bio-inspired surfaces such as lotus leaves, fish scales, and butterfly wings which requires the construction of micro-/nanohierarchical structures using molecular building blocks with low water affinity.[14–16] In this context several fabricated hydrophobic surfaces have been used as advanced sorbent materials for oil–water separation using fabrics, meshes, and foams to create hydrophobic–oleophilic substrates.[17–23] Mostly, artificial super-wetting surfaces become unstable due to the structural destruction after being utilized for absorption under various chemical and mechanical conditions continously.[24] Hitherto, the efforts to develop robust and superwetting surfaces have been primarily aimed at maintaining extremely textured assemblies with consistent chemical composition to maximize their practical applications. To strengthen the mechanical and chemical robustness of super-wetting surfaces, organosilicon and siloxane-based compounds have attracted extensive attention for the development of superhydrophobic hybrid materials.[25]

Polyhedral oligomeric silsesquioxane (POSS) is a remarkable hybrid material that integrates inorganic and organic components, represented by the chemical formula $RSiO_{1.5}$ and it features a distinctive three-dimensional cage-like structure with dimensions spanning from nearly 1 to 3 nm.[26,27] The POSS nanocages comprise Si–O bonds with silicon atoms positioned at the eight corners of a cube, connected by oxygen atoms and adorned with eight organic groups, a unique structure that confers hydrophobic properties and enhances their solubility in most organic solvents.[28] In addition, the non-toxic silica core enhances the material's rigidity and thermal stability, giving POSS exceptional durability. Unlike organic compounds, POSS is distinguished by its odorless and eco-friendly nature, attributed to the absence of volatile organic byproducts during reactions, made possible by its non-toxic silica core. Consequently, the organic groups attached to the POSS cage serve as reactive sites for subsequent functionalization, thereby making POSS an excellent choice as a starting material.[29–32] The functionalized POSS has been attached on the surface of substrates (cotton fabric and mesh) and combined with polymers, metal–organic frameworks and graphene *via* covalent or non-covalent bonding, resulting in enhanced dispersion ability, improved thermal stability, increased mechanical strength, and unique surface properties including superhydrophobicity. In the process of modifying substrate surfaces, superhydrophobic cotton fabrics and copper mesh were created by reacting functionalized substrates with functionalized POSS through covalent modification such as click and hydrolysis reactions.[33,34] These improved substrates are then used for applications such as self-cleaning and oil/water separation. In POSS–polymer composite materials, superoleophobic F-POSS/PMMA,[35] superomniphobic F-POSS/PDMS[36] and superhydrophobic F-POSS/PEGDA,[37] as well as Ph-a7b3-POSS/PIM[38] and F-POSS/APP/bPEI[39] were synthesized by blending functionalized POSS with their respective polymers and were employed for applications of self-cleaning and oil/water separation. In POSS/MOF materials, aminopropyl isooctyl polyhedral oligomeric silsesquioxane has been employed to selectively modify copper trimesate ($Cu_3(BTC)_2$) by attaching the POSS to the unsaturated copper sites on its outer surface, therefore it improves stability against humidity by generating a hydrophobic environment.[40] Our group reported the superhydrophobic ZIF-POSS material with a WCA of 157° achieved through post-covalent modification of ZIF-90 with POSS-NH_2 and a hydrophobic Ph-POSS@HKUST-1 composite with a WCA of 137 ± 4° obtained by the *in situ* growth of HKUST-1 with Ph-POSS.[41] Both ZIF-POSS and Ph-POSS@HKUST-1 were utilized as sorbent materials for oil and organic solvents. Nevertheless, there is a scope for utilization of POSS over various supports towards improved oleophilic properties.

Next-generation carbon-based 2D nanomaterials, including graphene and graphene oxide (GO), have garnered substantial consideration owing to their unique structural properties such as surface area, reactivity, and exceptional mechanical strength.[42] The covalent functionalization of GO with POSS provides an excellent platform for generating a new hybrid material POSS–graphene with multiple functionalities. The solution-cast POSS–graphene films unequivocally exhibit superhydrophobic properties, boasting a water/air contact angle of about 157°. Additionally, the superhydrophobic POSS–graphene powder was suitable for constructing liquid marbles.[43] Tang *et al.* reported the conversion of hydrophilic GO sheets into superhydrophobic GO-ePOSS materials through an esterification reaction of GO with epoxy-polyhedral oligomeric silsesquioxane (ePOSS) and demonstrated the effectiveness of GO-ePOSS membranes for efficient oil–water separation.[44] Among several graphene derivatives, fluorinated graphene (FG) containing C–F covalent bonds, due to its high WCA of 164 ± 6° and super-wetting nature when combined with diverse materials, was utilized for sorption/separation and self-cleaning applications.[45–47] Datta *et al.* reported the *in situ* growth of HKUST-1 on FG nanosheets, achieving a WCA of 147°, as well as the development of superhydrophobic ZIF-7 and ZIF-11 on FG nanosheets, specifically for oil–water separation.[48] However, to date there are no reports on the utilization of FG as a support for the growth of POSS from precursors using the *in situ* approach. Inspired by the above research, we have established the *in situ* growth of octaphenyl POSS on fluorinated graphene sheets by hydrolytic condensation of phenyl triethoxysilane. The resulting O-Ph-POSS-FG composite shows a WCA of 152 ± 2° with a surface free energy of ~5.6 mJ m^{-2}. The as-synthesized O-Ph-POSS-FG was confirmed by FT-IR spectroscopy, PXRD, SEM, TEM, TG analysis, ^{29}Si NMR spectroscopy, N_2 adsorption–desorption isotherms and XP spectroscopy. The superhydrophobic O-Ph-POSS-FG composite

demonstrated excellent chemical and thermal stability and was further coated on a polyurethane sponge to create O-Ph-POSS-FG@Sponge. The resulting sponge exhibits exceptional selective sorption of oils and organic solvents, with a sorption capacity ranging from 1500 to 5500 wt% and a separation efficiency of 90–99%, with excellent chemical stability along with multiple reusabilities.

Experimental section

Materials and methods

All reagents and solvents were obtained commercially in reagent-grade quality and used as received, without any further purification. Phenyl triethoxysilane (PTES) and fluorinated graphite ($C_1F_{1.1}$) were purchased from Alfa Aesar and Sigma Aldrich, respectively. Potassium hydroxide (KOH) is supplied by Fisher Scientific and a commercially available polyurethane sponge was used. Fourier transform infrared (FT-IR) spectra were recorded using a Shimadzu IR Tracer-100 in the range of 400–4000 cm^{-1}, with the sample powder pressed into a pellet with KBr, while the crystallinity of the composites was measured using a powder X-ray diffractometer (PXRD) from PANalytical India, Spectris Technologies, employing Cu Kα radiation (λ = 1.54 Å) within the range of 5 to 60°. Solid-state ^{29}Si NMR results were obtained from a Bruker Avance DPX-250 spectrometer. The morphology of the composite was observed using a field emission scanning electron microscope FEI QUANTA 200 and a transmission electron microscope, JEM-2100 Plus microscope JEOL (Japan). Thermogravimetric analysis (TGA) of the composite was carried out on a Netzsch-STA 2500 Regulus instrument under N_2 gas, while X-ray photoelectron spectroscopy (XPS) data were recorded on ULVAC-PHI, PHI5000 Version Probe III equipment from Physical Electronics. The composite's surface area was measured using a BET Quantachrome Autosorb iQ sorption analyzer. The contact angle meter (sessile drop) KYOWA DMs-40 was used to test the wetting behaviors of the composite with water and solvents, and the half-angle method fitting and FAMAS Add-in software were used, with a solvent droplet range of 2–10 μL. Kitazaki Hata theory was used to calculate the solid surface free energy of the samples by measuring the contact angle of three probe liquids, water, ethylene glycol, and hexadecane. The surface topography and roughness factor were assessed with an atomic force microscope (AFM, Park Systems Corporation, XE7). The topographical measurement was performed in the conventional contact mode. Total organic carbon (TOC) determination was performed with the High-Performance TOC Analyzers multi N/C UV HS (Analytik Jena AG, Germany) equipped with the HT 1300 furnace module.

Synthesis of O-Ph-POSS-FG

60 mg of fluorinated graphite was added to 20 ml toluene and sonicated for 3 h to obtain exfoliated fluorographene sheets. A solution of 1.8 ml PTES in toluene (20 ml) was placed in an RB flask with 0.5 g of KOH under an inert atmosphere. The above mixture was refluxed at 110 °C until KOH dissolved. Then the sonicated mixture of FG in toluene was transferred into the reaction mixture with the addition of 0.5 ml of water, with the temperature maintained at 110 °C. The reaction mixture was continued to reflux for 12 h. After 12 h, the product was obtained by centrifugation. The obtained solid was washed with absolute ethanol and methanol three times and dried at 70 °C overnight. The yield was 0.644 g.

Preparation of O-Ph-POSS-FG@Sponge

O-Ph-POSS-FG@Sponge was prepared by dip-coating. 100 mg of O-Ph-POSS-FG were dispersed in methanol (60 ml) by sonication. Commercially available polyurethane sponges were cut ($1 \times 1 \times 1$ cm^3) and washed with deionized water and dried completely. Five cut PU sponges were dip-coated in the composite solution, and the coated sponges were dried at 80 °C for 12 h.

Preparation of oil in water and water in oil emulsion solutions

Preparation of oil in water emulsion. For an emulsion of toluene in water, 5 ml of toluene was added to 45 ml of water and 2.5 mg of sodium dodecyl sulfate was added and allowed to stir at 1000 rpm for 5 h. A milky white toluene in water emulsion was obtained.

Preparation of water in oil emulsion. Similarly, for an emulsion of water in toluene, 5 ml of water and 45 ml of toluene followed by 2.5 mg of sodium dodecyl sulfate were added and allowed to stir at 1000 rpm for 5 h. A milky white water in toluene emulsion was obtained.

Results and discussion

Synthesis and characterization

We report the *in situ* growth of octaphenyl POSS over the multi-layered FG sheets *via* non-covalent interactions between the phenyl group and fluorinated graphene nanosheets (Scheme 1). The ultrasonication of bulk fluorinated graphite in toluene produces multilayer FG nanosheets. The hydrolysis of phenyl triethoxysilane over the multilayer FG nanosheets in the presence of KOH and water medium produces silanol monomers that form triol monomers which are unstable and further undergo condensation to produce octaphenyl cubic POSS over the multilayer FG nanosheets. The formation of the O-Ph-POSS-FG nanocomposite was confirmed by FT-IR spectroscopy, PXRD, SEM, TEM, TG analysis, ^{29}Si NMR spectroscopy, N_2 adsorption–desorption isotherms and XP spectroscopy. Additionally, the wetting behavior and SFE of the O-Ph-POSS-FG nanocomposite were studied by water/solvent contact angle analysis.

The FT-IR spectrum of the O-Ph-POSS-FG composite is displayed in Fig. 1a. The IR bands at 1086, 1021, and 520 cm^{-1} are ascribed to the characteristic Si–O vibrations of the silsesquioxane framework in O-phenyl-POSS. Additionally, the characteristic peak at 3026 cm^{-1} corresponds to the asymmetric stretching of C–H bonds, the peaks between 1400 and

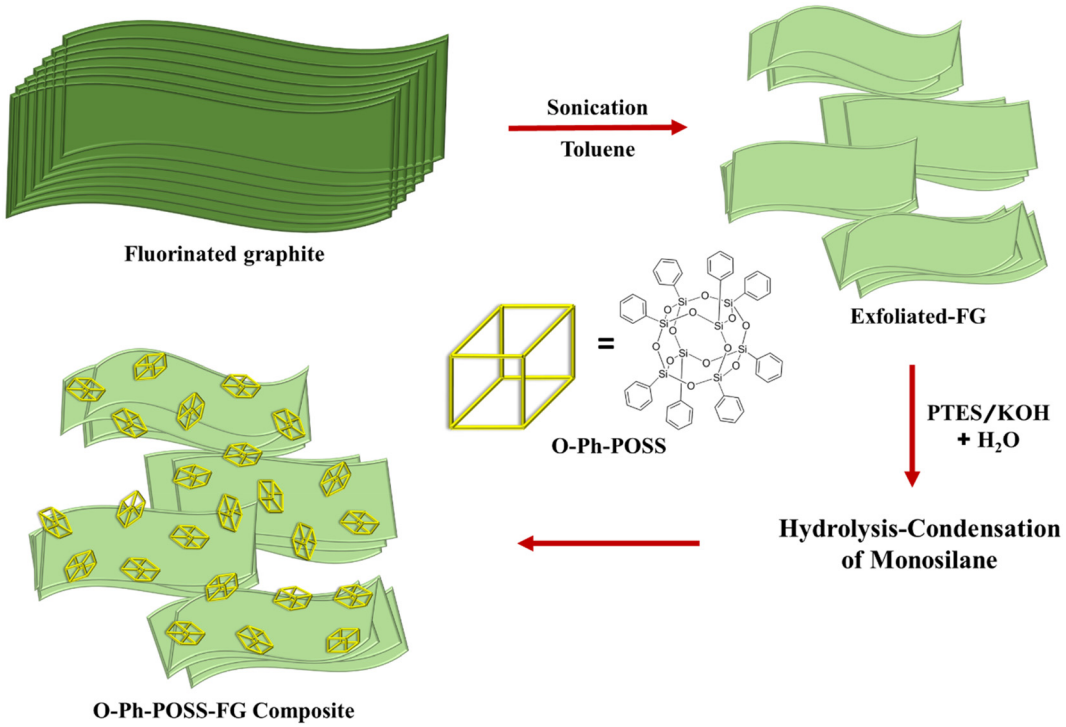

Scheme 1 Synthesis of the O-Ph-POSS-FG composite.

1600 cm^{-1} correspond to the stretching vibrations of the C=C bonds, and the signals at 695 and 735 cm^{-1} correspond to the out-of-plane deformation of C–H in the phenyl groups.[29,49] The characteristic peak at 1206 cm^{-1} corresponds to the FG nanosheets due to the covalent C–F bonds.[48] These results suggest that O-Ph-POSS has been effectively assembled over the FG *via in situ* growth.

As inferred from the PXRD pattern of O-Ph-POSS-FG (Fig. 1b), it is clear that all the peaks of the as-synthesized O-Ph-POSS-FG match those of O-Ph-POSS reported in the literature.[50] The diffraction peaks of O-Ph-POSS-FG at 2θ values ~8.2°, 10.7°, 18.4°, 19.9°, and 24.9° correspond to reflection planes (100), (110), (001), (120), and (022) suggesting the successful formation of rhombohedral crystals of O-Ph-POSS over the fluorinated graphene multi-layers. These results confirmed that the hydrolytic condensation of phenyl triethoxysilane in alkaline medium supported over FG multi-layers led to the formation of cubic O-Ph-POSS nanocages. The morphology of the O-Ph-POSS-FG composite was studied by FE-SEM and TEM as shown in Fig. 1c and d. The SEM image (Fig. 1c) shows the accumulation of the cubic O-Ph-POSS nanocages dispersed on FG multi-layered sheets. The TEM image (Fig. 1d) displayed the dispersion of cubic O-Ph-POSS nanocages supported over the edges of few-layered FG nanosheets comparable to existing works,[48,51] indicating the stabilizing role of FG in the growth of O-Ph-POSS.

The thermal behavior of O-Ph-POSS-FG was investigated using TGA by heating the sample at a consistent rate of 10 °C min^{-1} under a nitrogen atmosphere. The weight loss of the O-Ph-POSS-FG composite takes place in two stages; where the initial weight loss of approximately 8% in the temperature range of 100–400 °C corresponds to the gradual detachment of phenyl groups from O-Ph-POSS. The major weight loss of about 45% in between the temperatures of 420–600 °C is observed because of the detachment of fluorine from the FG nanosheets and further conversion of the cubic silsesquioxane framework into silica (Fig. 2a). The solid-state ^{29}Si NMR spectrum of the O-Ph-POSS-FG composite displays a single signal at −77.7 ppm as shown in Fig. 2b, characteristic of the eight silicon atoms in the same environment, matching the previously reported O-Ph-POSS.[52] From this single peak, it is evident that the *in situ* growth of silicon monomers on the FG sheets facilitates the formation of cubic O-Ph-POSS nanocages rather than other polymeric structures of POSS. This result indicates the formation of a completely condensed oligomeric phenyl silsesquioxane[53] with eight equivalent silicon atoms over FG sheets. N_2 adsorption isotherms were used to measure the surface area of the as-synthesized O-Ph-POSS-FG nanocomposite, which showed a type-I isotherm (Fig. S1†) with a surface area of 64 m^2 g^{-1} and the pore-size distribution revealed two kinds of pores predominantly in the micropore regime along with the existence of minimal mesopores. The development of micro/meso pores can originate due to the formation and assembly of POSS over few-layered FG nanosheets. The topography of the material surfaces was measured by atomic force microscopy[54] and the obtained results for the O-Ph-POSS-FG material revealed that the particles have a height of 0.4 μm, with an average surface roughness (R_a) of 54 nm and a roughness factor (R) of 1.10 (Fig. S2†).

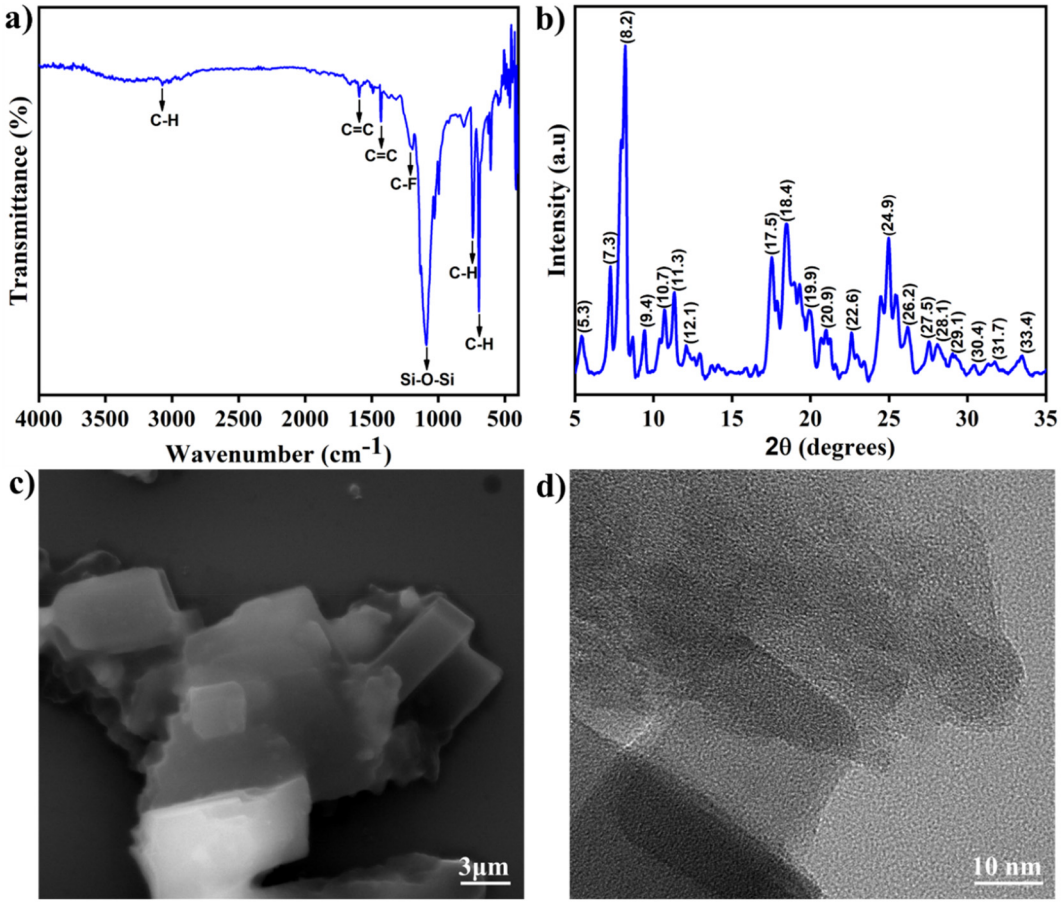

Fig. 1 (a) FT-IR spectrum, (b) PXRD pattern, (c) FE-SEM image and (d) TEM image of O-Ph-POSS-FG.

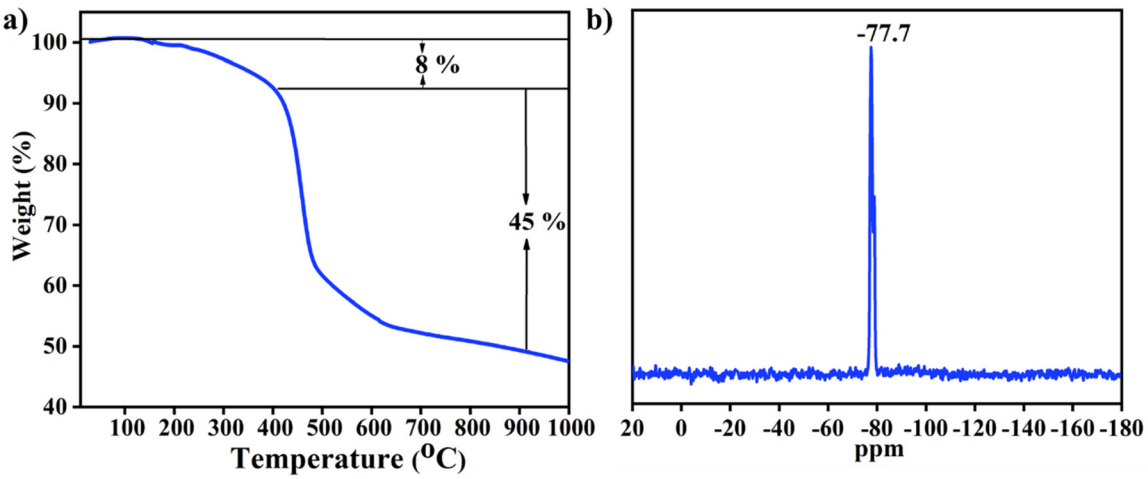

Fig. 2 (a) Thermogravimetric analysis and (b) solid-state ^{29}Si NMR spectrum of O-Ph-POSS-FG.

The presence of the elements and the binding energies are studied from the survey scan of the XP spectra of O-Ph-POSS-FG. The survey scan reveals the peaks conforming to C 1s, O 1s, F 1s, Si 2s, and Si 2p associated with the O-Ph-POSS composite, as shown in Fig. 3a. The C 1s spectrum shows the functionalities corresponding to both the O-Ph-POSS and FG. The high-resolution C 1s spectra of the composite display five distinct peaks assigned to the C═C, C–C, Si–C, CF–CF_2, and C–F_3 bonds positioned at 284.3, 284.8, 285.1, 290.4, and 293.2 eV respectively as shown in Fig. 3b. In Fig. 3c, the binding

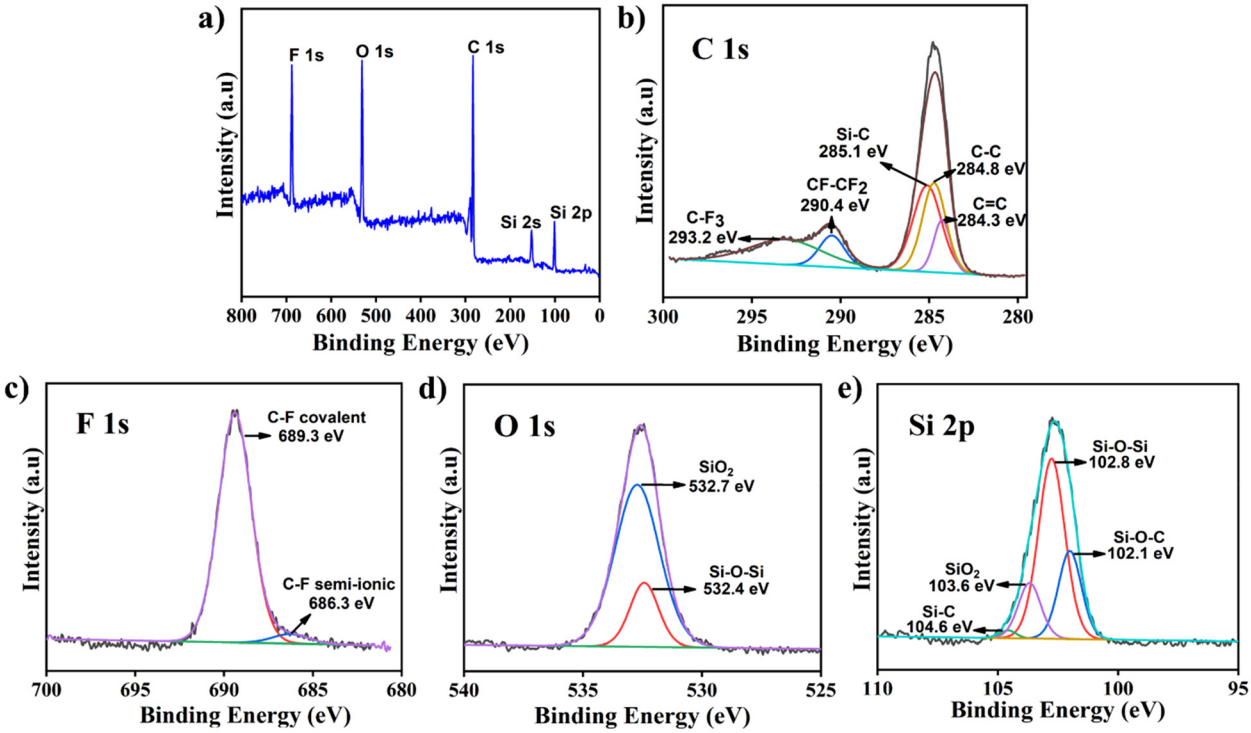

Fig. 3 XPS (a) survey spectrum; and slow scans of (b) C 1s, (c) F 1s, (d) O 1s, and (e) Si 2p of the O-Ph-POSS-FG composite.

energies at 689.3 and 686.3 eV occur from the FG sheets assigned to the F 1s with respect to majority of C–F covalent and minor C–F semi-ionic bonding respectively. The peaks around 532.4 and 532.7 eV from the O 1s and the high-resolution Si 2p peaks at 102.1, 102.8, 103.6, and 104.6 eV corresponding to Si–O–C, Si–O–Si, SiO_2, and Si–C bonds originated from O-Ph-POSS (Fig. 3d and e). These results further indicate the formation of O-Ph-POSS on the FG multi-layers.

The wettability of the as-prepared O-Ph-POSS-FG was evaluated by solvent contact angle measurements. The O-Ph-POSS-FG shows a WCA of about 152 ± 2° indicating that O-Ph-POSS-FG is superhydrophobic in nature. This is mainly due to the presence of organic groups on POSS linked to the fluorinated graphene multi-layers. In addition, the wetting behavior of O-Ph-POSS-FG was studied by introducing water and oil droplets onto the surface of the material. In comparison, the water and oil droplets were displaced on the surface of the O-Ph-POSS-FG, and the water acquires spherical shape, whereas the oil droplets wetted the surface completely as shown in Fig. 4a and b. Ethylene glycol and hexadecane solvents were selected, and the respective contact angles' and the surface free energy (SFE) analysis of the O-Ph-POSS-FG composite was investigated. In addition to C–F linkages, each POSS cage's eight bulky phenyl groups, grown on the FG nanosheets, showed an ethylene glycol contact angle of 144 ± 2°, whereas hexadecane wetted the powder (Fig. 4c). The surface free energy of O-Ph-POSS-FG was determined to be 5.6 mJ m^{-2} based on the wetting capacities of three distinct solvents. Additionally, the stability of water droplets on O-Ph-POSS-FG was assessed by recording the contact angle values for up to 30 minutes during kinetic measurement. It is noteworthy that O-Ph-POSS-FG remained hydrophobic even after 30 minutes by maintaining a substantially identical WCA, from 152 to 149° (Fig. 4d). These findings suggest that the hydrophobic nature of the O-Ph-POSS-FG composite is persistent. It is important to note that the slight reduction in WCA comes from the slow interaction of the dispensed water moieties with the Si–O–Si group of the O-Ph-POSS-FG material.

A commercially available, inexpensive, and macroporous polyurethane sponge is the preferred host matrix for attaching the O-Ph-POSS-FG material, and it can also be used for recycling processes. The dip-coating of the O-Ph-POSS-FG material onto a PU sponge (1 × 1 × 1 cm^3) produces the O-Ph-POSS-FG@Sponge. The PU sponge and O-Ph-POSS-FG@Sponge are shown in Fig. S3.† The density and porosity of the pristine sponge as well as O-Ph-POSS-FG@Sponge were measured. The uncoated sponge has an average density of 0.0601 g cm^{-3} and an average porosity of 99%. The O-Ph-POSS-FG coated sponge gives an average density of 0.0782 g cm^{-3} and average porosity of 98.6 ± 0.1% and the results are given in Table S1.† The O-Ph-POSS-FG@Sponge displays a WCA of about 151 ± 2° indicating that the O-Ph-POSS-FG@Sponge is superhydrophobic in nature (Fig. S4†). The weather resistance of O-Ph-POSS-FG@Sponge, prepared at different time intervals (1 week and 1 year prior), was evaluated through water contact angle measurements. The WCA values obtained for the aged samples were found to be comparable to those of the freshly prepared O-Ph-

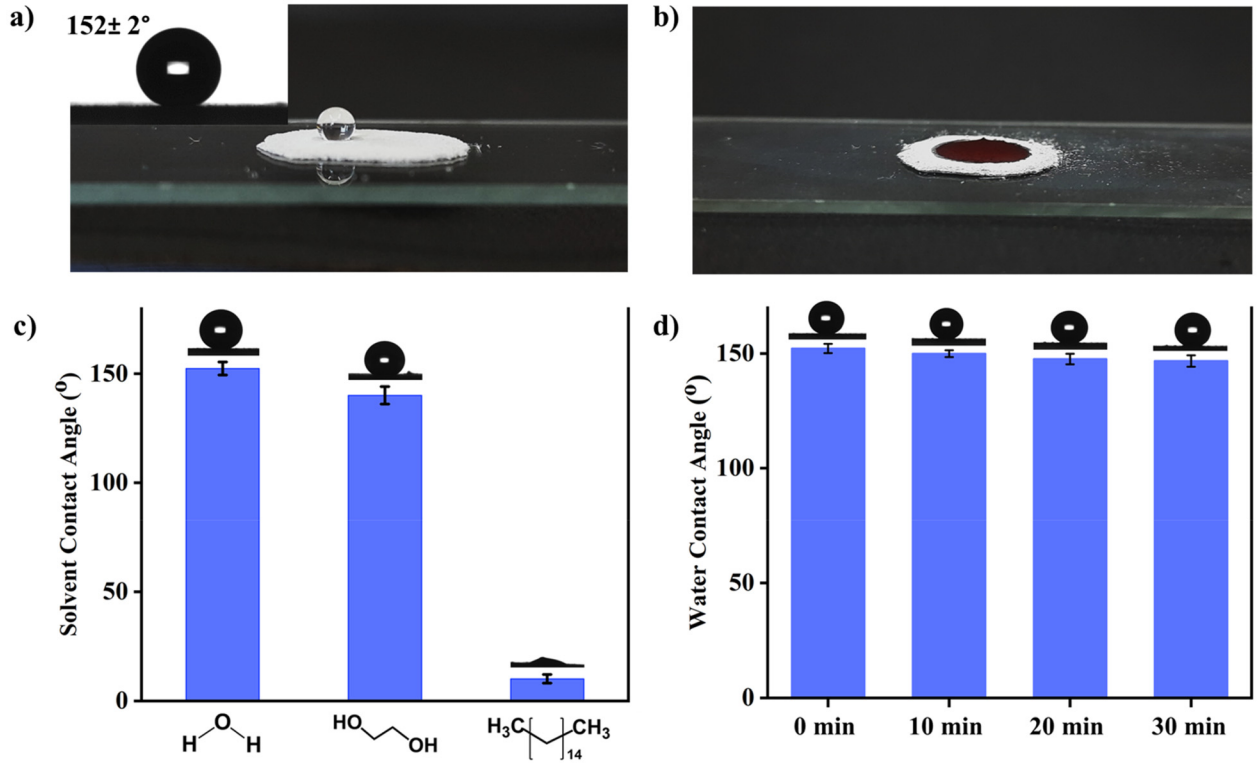

Fig. 4 Wetting behavior of O-Ph-POSS-FG on (a) water, with the water contact angle shown in the inset, and (b) silicone oil; (c) plots of solvent contact angles for water, ethylene glycol, and hexadecane on O-Ph-POSS-FG; (d) WCA kinetics measured every 10 minutes for O-Ph-POSS-FG.

POSS-FG@Sponge (Fig. S5†). These results demonstrate that the O-Ph-POSS-FG@Sponge exhibits excellent weather resistance, maintaining its performance over extended periods.

To assess the mechanical stability of O-Ph-POSS-FG@Sponge, it is crucial to ensure that its hydrophobic properties are maintained under continuous physical deformation. The mechanical stability of the O-Ph-POSS-FG@Sponge was evaluated by measuring the water contact angle following various physical treatments including tape peeling, knife cutting, rubbing with emery paper, and compression under load (Fig. S6†). The superhydrophobic behavior of the physically deformed O-Ph-POSS-FG@Sponge was then measured and compared to that of the untreated sponge. Among the different treatments, the tape-peeling O-Ph-POSS-FG@Sponge exhibited a WCA of 151 ± 2°, while the knife-cut sponge showed a slight reduction in WCA to 150 ± 2°. The sponge subjected to rubbing with emery paper retained a WCA of 151 ± 2°. These results demonstrate that the O-Ph-POSS-FG@Sponge maintains excellent mechanical stability and superhydrophobic properties, even after undergoing various physical deformations.

The modified O-Ph-POSS-FG@Sponge floated completely on the water surface but the PU sponge sank due to its hydrophilicity (Fig. S7†). The roughness and interconnected channels in the uncoated PU material promote capillary action, drawing water in and enhancing wettability, which leads to a lower apparent contact angle. To evaluate the absorbency of the O-Ph-POSS-FG and O-Ph-POSS-FG@Sponge, we explored a variety of organic solvents and oils. The absorption capacity of O-Ph-POSS-FG, summarized in Fig. 5a, ranges from 200 to 500 wt%, with chloroform exhibiting the maximum capacity at 500 wt%, hydrocarbons showing approximately 200–250 wt%, and hexane having the lowest capacity at 200 wt%. The highest and lowest absorption capacities of the hydrophobic-oleophilic O-Ph-POSS-FG@Sponge are 5500 wt% for chloroform and 1500 wt% for coconut oil respectively (Fig. 5b). As shown in Table S2,† O-Ph-POSS-FG@Sponge demonstrated absorption capacities and separation efficiencies for oils and various organic solvents that are comparable to those reported for functionalized POSS and graphene composites.

The superhydrophobic nature of the O-Ph-POSS-FG@Sponge is vital for the practical application of separation of organic solvents and oil pollutants from water mixtures. As shown in Fig. 6, the O-Ph-POSS-FG@Sponge was placed in a mixture of hexane and water and placed over the surface to absorb hexane dyed with oil red O; only clean water was left in the beaker. In this experiment, 10 ml water and 5 ml (ratio 2 : 1) organic solvent or oil were used for each experiment, the coated O-Ph-POSS-FG@Sponge absorbed the selective solvents and oils, organic solvents were absorbed completely within 10 s and oil was absorbed in 20 s due to their density. In addition, a similar experiment was carried out for the separation of dense chloroform from a mixture of chloroform and water, where the O-Ph-POSS-FG@Sponge was

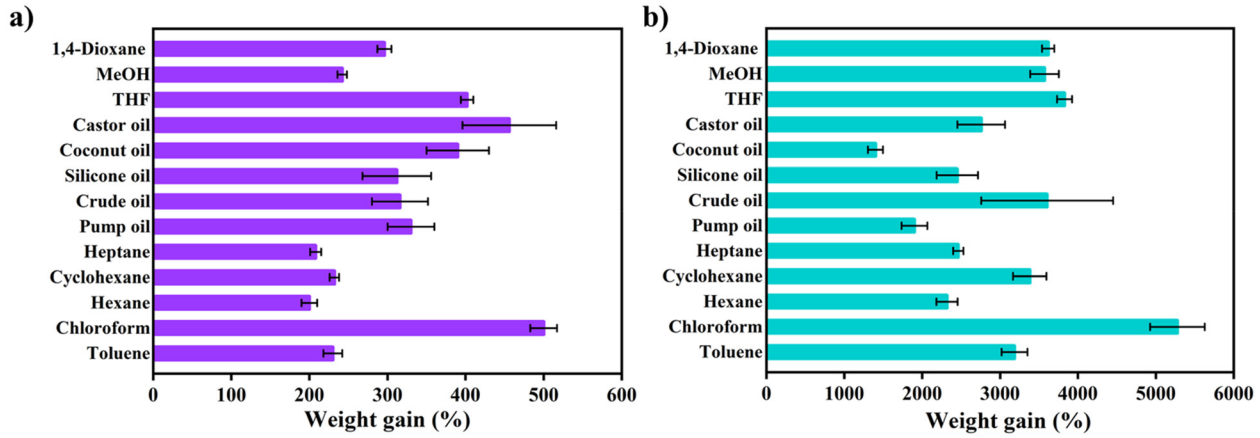

Fig. 5 (a) Solvent absorption capacity of the O-Ph-POSS-FG composite; (b) absorption capacity of O-Ph-POSS-FG@Sponge.

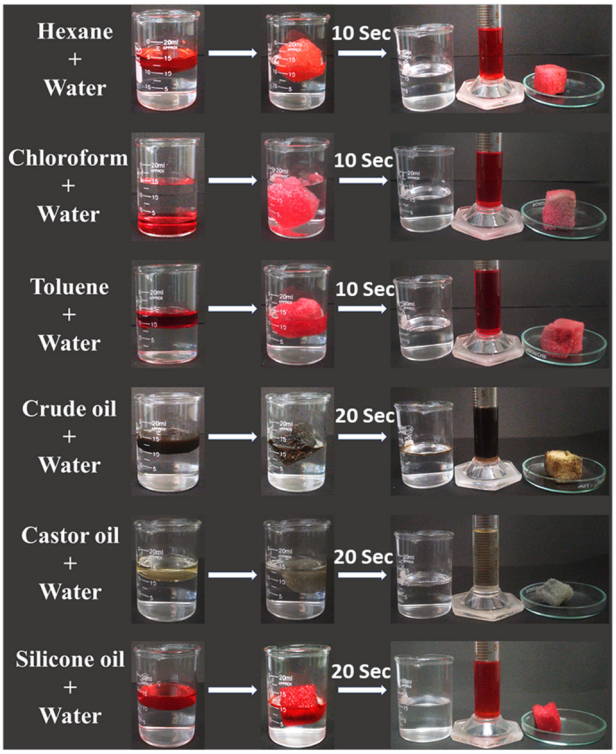

Fig. 6 Solvents and oils separation from water mixtures using O-Ph-POSS-FG@Sponge. For clarity the organic solvent is colored with Oil Red O.

moved to the bottom of the water. Chloroform was completely absorbed from the underwater rapidly. This selective separation further demonstrates the potential of O-Ph-POSS-FG@Sponge for cleaning up different oil spills from the variety of oil and water mixtures. As shown in Fig. 7a, the separation efficiency of the O-Ph-POSS-FG@Sponge with a variety of organic solvent/water mixtures and oil/water mixtures was studied using a 1 : 1 ratio of solvent to water. O-Ph-POSS-FG@Sponge absorbed complete solvents and oils from the water mixture and the absorbed liquids were removed *via* swelling–squeezing and solvents were collected with high efficiency in the range of 90 to 99%. After the sorption of various solvents from hexane/water, chloroform/water, toluene/water and cyclohexane/water mixtures, both the recovered solvents and the O-Ph-POSS-FG@Sponge were analyzed using FT-IR spectroscopy (Fig. S8†). The FT-IR spectra of the recovered solvents were found to be consistent with those of the pure solvents, and the recovered O-Ph-POSS-FG@Sponge exhibited identical features to the untreated O-Ph-POSS-FG@Sponge. These results strongly indicate that the O-Ph-POSS-FG@Sponge did not undergo leaching during contact with the organic solvents. Additionally, FT-IR analysis confirmed the absence of O-Ph-POSS-FG functionalities in the recovered solvents, further supporting the integrity of the material during the separation process. Therefore, no secondary waste is generated during the separation process. We have conducted a total organic carbon (TOC) analysis to evaluate the oil content in the filtrate before and after the separation of an oil-in-water mixture. The TOC value for commercial n-hexane was measured at 18.2 ppm, while the TOC value of the recovered *n*-hexane, after separation from the *n*-hexane/water mixture, was 17.5 ppm. Similarly, for chloroform, the TOC value for the pure solvent was 25.8 ppm, and the TOC value for the recovered chloroform was 24.7 ppm. These results suggest that trace amounts of water remain in the recovered solvents following the separation process. From Fig. S9,† the flux recovery ratio (FRR) and irreversible fouling ratio (RIR) of O-Ph-POSS-FG@Sponge were analyzed for both organic solvents and oils. The results demonstrated that the O-Ph-POSS-FG@Sponge exhibited excellent performance in absorbing various oils and organic solvents, with FRR values ranging from 80% to 92% and RIR values ranging from 8% to 20%. These findings highlight the material's efficient recovery and low susceptibility to irreversible fouling during the separation process.

Furthermore, the reusability of O-Ph-POSS-FG@Sponge was verified through the separation of hexane from the hexane/

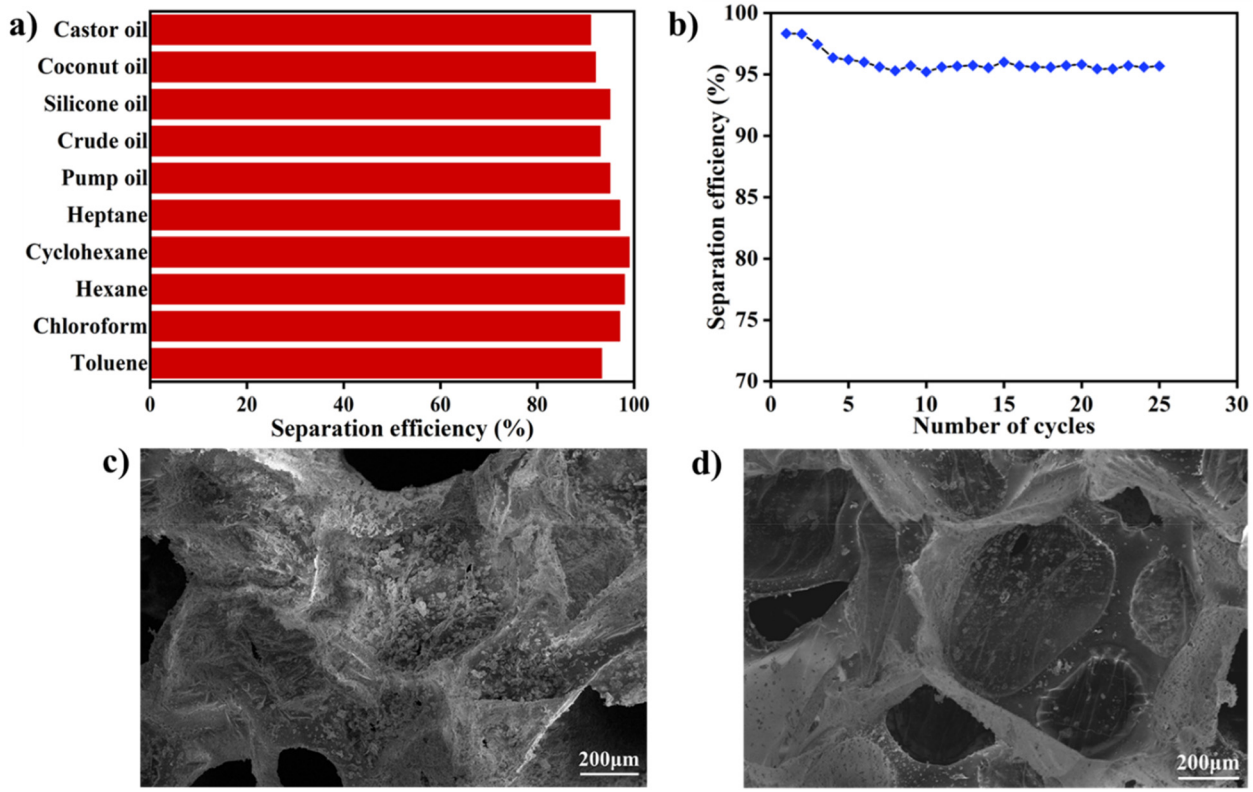

Fig. 7 (a) Separation efficiency of O-Ph-POSS-FG@Sponge; (b) reusability test of O-Ph-POSS-FG@Sponge; (c) SEM images of O-Ph-POSS-FG@Sponge and (d) O-Ph-POSS-FG@Sponge after 25 cycles of hexane-water separation.

water mixture. The sponge coated with the material was dried at 60 °C after each separation to remove the volatile hexane/chloroform. Subsequently, the same O-Ph-POSS-FG@Sponge was used for separation up to 25 times (Fig. 7b). The SEM images in Fig. 7c and d reveal that the used sponge maintained the same morphology as the freshly coated sponge, indicating that the coating effectively preserved the sponge's hydrophobicity. Furthermore, the O-Ph-POSS-FG@Sponge was tested for the separation of viscous liquids, including pump oil, over a series of 25 cycles. During the first 15 cycles, the sponge demonstrated an oil recovery efficiency of 98%. However, after the 20th cycle, the separation efficiency gradually decreased to 88% (Fig. S10†). This decline in performance is attributed to the accumulation of residual pump oil in the sponge during repeated use, which likely impacted its ability to achieve optimal separation efficiency in subsequent cycles.

The chemical stability of O-Ph-POSS-FG and O-Ph-POSS-FG@Sponge was carried out to confirm their application in acidic and alkaline solutions. The hydrophobic properties of both O-phenyl-POSS-FG and O-phenyl-POSS-FG@Sponge effectively prevent the entry of aqueous solutions across a broad pH range. This indicates that there is no leaching of the O-phenyl-POSS-FG material into the solution, and the color of the sponge remains unchanged (Fig. S11 and S12†). POSS is known to be non-toxic and highly biocompatible, whereas fluorinated graphene nanosheets act as a support towards POSS particles. Compared to perfluoro organic compounds, fluorinated graphite due to its network structures shows no fluoride leaching and non-toxic behaviour. Additionally, SEM images reveal that the morphology of the O-phenyl-POSS-FG coated sponge remains intact, with no damage to the PU fibres following acid and alkaline treatments (Fig. S13†). The floatability of the O-Ph-POSS-FG@Sponge was observed in acidic, alkaline, sea and normal water with toluene as a solvent. The O-Ph-POSS-FG@Sponge selectively absorbs toluene within 10 seconds (Fig. S14†). Importantly, the sponge floats in water after the absorption of toluene. The sponge was kept over a period of more than 2 hours, during which the solvent on the upper surface gradually evaporated, facilitating solvent recovery.

The O-phenyl-POSS decorated over the fluorinated graphene sheets contains a thermally and chemically stable Si–O–Si core with eight phenyl groups covalently bonded with a POSS skeleton providing hydrophobicity and oleophilicity. Furthermore, the synergistic interaction between the FG multilayers and POSS nanocages enhances absorption properties, as well as thermal and chemical stability. This combination improves the selectivity and separation efficiency of the O-Ph-POSS-FG composites for a variety of organic solvents and oils.

We probed the toluene sorption under supercool/superheat conditions. For the supercool conditions, a toluene/water mixture was placed in a chiller at −40 °C for one hour before being used for separation with O-Ph-POSS-FG@Sponge. The sponge successfully separated approximately 87% of the toluene

from the supercooled toluene/water mixture. In contrast, to simulate superheat conditions, the toluene/water mixture was heated to 100 °C and used for separation studies with O-Ph-POSS-FG@Sponge. Under these conditions, a separation efficiency of 76% was achieved (Fig. S15†). The reduced sorption efficiency under superheated conditions is attributed to the slight evaporation of toluene at the elevated temperature, which likely contributed to the diminished separation performance.

The separation of oil from an oil/water mixture was carried out by choosing the O-Ph-POSS-FG@Sponge with dimensions of (1 × 1 × 1 cm^3), resulting in a surface area or effective contact area (A) of 0.0001 m^2 for two solvents such as toluene and chloroform with different densities. The resultant sponges were connected to a substrate holder which was subsequently fixed to a vacuum pump (Model TID-25-P, Flow 25 L min^{-1}, Max. Vacuum: 22 inches Hg, motor 1/16 HP operated at 230 V) to create a pressure-driven flow for selective organic separation. The separation was done by taking 25 mL of solvent in 200 mL of water (Fig. 8). Toluene and chloroform were continuously infiltrated through the O-Ph-POSS-FG@Sponge and the recovered organics were collected in a flask in 40–65 s (Videos S1 and S2†). The flux (J) of toluene and chloroform through the O-Ph-POSS-FG@Sponge was calculated using the following formula:

$$J = \frac{V}{A \times T}$$

where J is the oil flux (L m^{-2} h^{-1}), V is the total volume of the collected oil (L), A is the effective contact area of the sponge with oils (m^2), and T is the operation time (h).

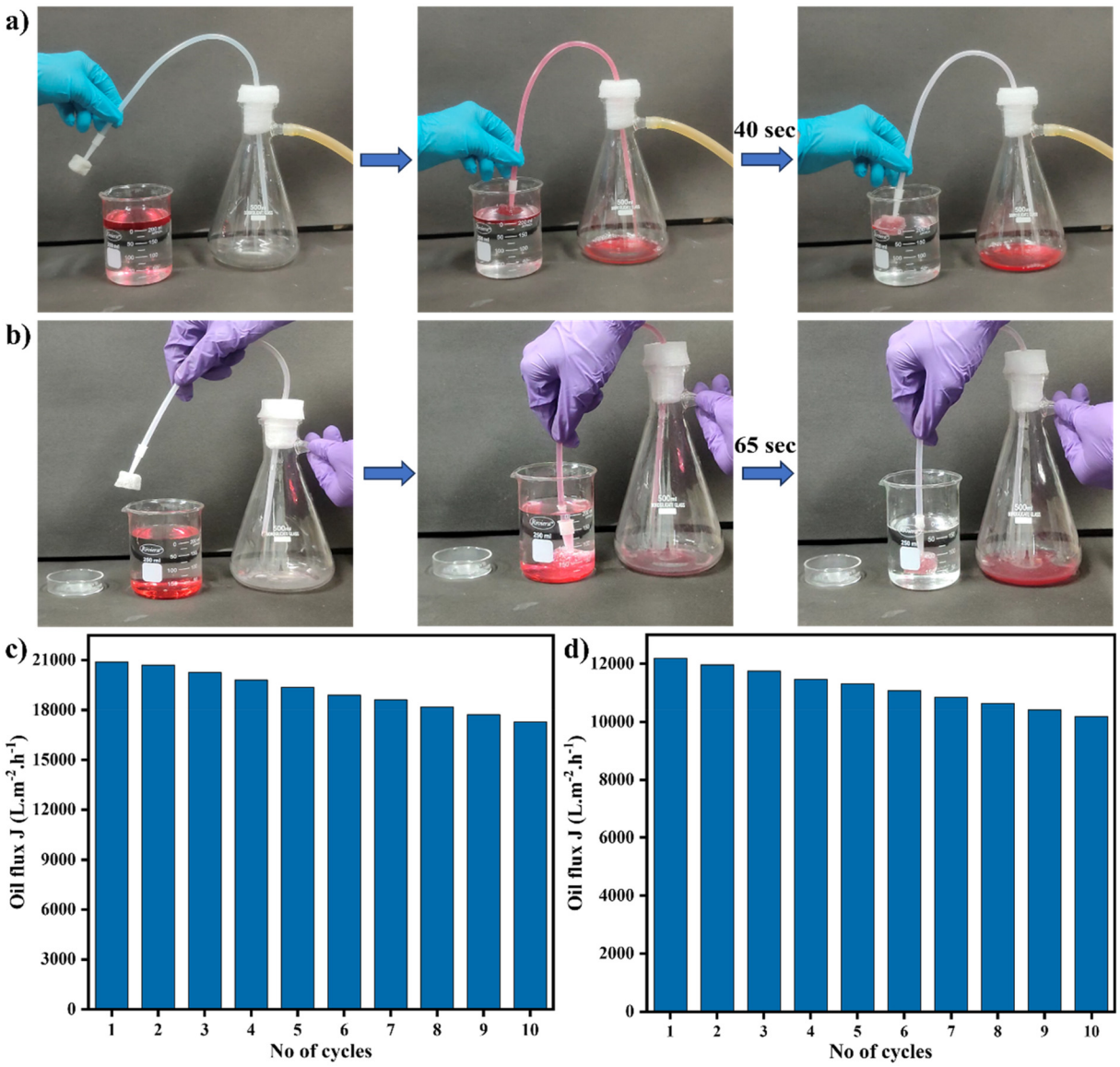

Fig. 8 Photographs of the continuous separation of (a) toluene and (b) chloroform from solvent/water mixture by O-Ph-POSS-FG@Sponge using a vacuum pump and the corresponding plots of flux for (c) toluene and (d) chloroform up to 10 cycles.

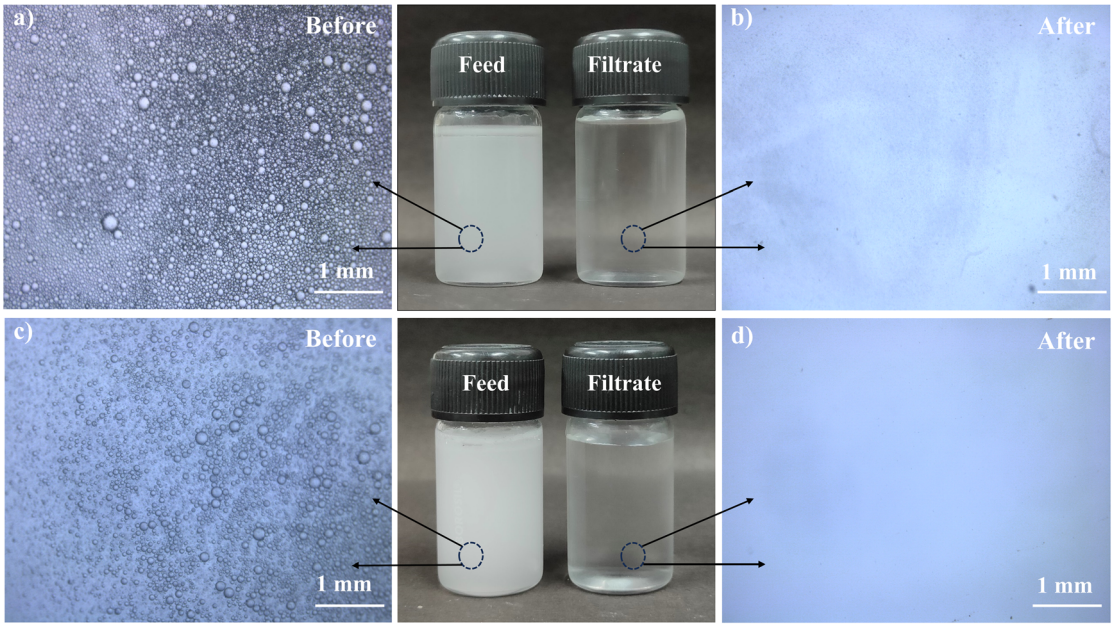

Fig. 9 Comparison of optical microscopic images before and after separation of (a and b) toluene-in-water and (c and d) water-in-toluene emulsions with surfactant and the process of particle size distribution of the emulsion.

The toluene and chloroform fluxes were 20 880 and 12 184 L m^{-2} h^{-1}, which considerably reduced over multiple reuse cycles as the solvent remains over the O-Ph-POSS-FG@Sponge. The fluxes of various organic solvents for O-Ph-POSS-FG@Sponge are comparable to those reported graphene-based composite materials.[55]

We have studied the separation performance of oil-in-water (O/W) and water-in-oil (W/O) emulsions using O-Ph-POSS-FG@Sponge. The water droplet size distribution was analyzed using optical microscopy images, before and after separation for toluene-in-water emulsion (Fig. 9a and b) and water-in-toluene emulsion (Fig. 9c and d) stabilized by a surfactant. The results demonstrated that no droplets remained after the separation process for both emulsion types. These findings demonstrate the effectiveness of O-Ph-POSS-FG@Sponge in efficiently separating stabilized emulsions, confirming its potential as a promising material for emulsion separation applications.

Conclusion

In conclusion, we have demonstrated the *in situ* growth of O-Ph-POSS nanocages over multi-layered fluorinated graphene nanosheets by the hydrolytic condensation reaction of phenyl triethoxysilane in the presence of potassium hydroxide. The results from FT-IR, PXRD, SEM, TEM, TG analyses, ^{29}Si NMR and XPS indicated that the O-Ph-POSS nanocages were successfully grown over exfoliated FG nanosheets. The resulting O-Ph-POSS-FG demonstrated superhydrophobic properties, featuring a water contact angle of 152 ± 2° and a surface free energy of 5.6 mJ m^{-2}. The O-Ph-POSS-FG has been developed for construction of a robust and hydrophobic–oleophilic surface by coating it over a PU sponge, which demonstrated a steady oil/organic absorption performance from oil/water mixtures with considerable separation even after 25 cycles and continuous separation of toluene and chloroform using a vacuum pump with fluxes ranging up to 20 880 and 12 184 L m^{-2} h^{-1} for toluene and chloroform respectively. The weather resistance of O-Ph-POSS-FG@Sponge, prepared at intervals of 1 week and 1 year, revealed that the aged samples retained similar WCA values to those of the freshly prepared sponge, demonstrating its excellent durability and long-term performance. The mechanical stability of the O-Ph-POSS-FG@Sponge demonstrated that the sponge retained its superhydrophobic properties, with WCA values of 151 ± 2° for tape peeling and emery paper and 150 ± 2° for knife cutting, demonstrating excellent stability despite deformation. In addition, utilizing the advantages of O-Ph-POSS with outstanding resistance, the prepared superhydrophobic O-Ph-POSS-FG exhibited excellent stability and durability after the separation of oil from the water mixture, besides under supercooled and heated conditions. Furthermore, optical microscopy analysis of the O/W and W/O emulsions, both stabilized by a surfactant, revealed that no droplets remained after separation, demonstrating the effectiveness of O-Ph-POSS-FG@Sponge and confirming its potential for emulsion separation applications. This study will endorse the widespread development of other superhydrophobic, chemically and mechanically robust interfacial materials using POSS.

Author contributions

Conceiving and designing the experiments: P. L., K. K. R. D. and S. S.; performing the experiments: P. L. and

A. C.; measuring and analyzing the data: P. L., R. Y., A. C., K. K. R. D. and S. S.; writing the manuscript: P. L., A. C., K. K. R. D. and S. S.

Data availability

The data will be made available from the authors upon considerable request.

Conflicts of interest

There are no conflicts to declare.

Acknowledgements

SS and PL gratefully acknowledge the financial support from the DST/SERB Government of India (CRG/2019/001254) and K. K. R. D. and R. Y. thank DST-SERB (ECR/2017/002075) for the financial support. All the authors thank DST-FIST, Department of Chemistry, Nanotechnology Research Centre and SRM IST, for PXRD and SEM facilities.

References

1 (*a*) L. Guterman, *Science*, 2009, **323**, 1558–1559; (*b*) M. Schrope, *Nature*, 2011, **472**, 152–154.
2 (*a*) Y. Cheng, X. Li, Q. Xu, O. Garcia-Pineda, O. B. Andersen and W. G. Pichel, *Mar. Pollut. Bull.*, 2011, **62**, 350–363; (*b*) H.-M. Choi and R. M. Cloud, *Environ. Sci. Technol.*, 1992, **26**, 772–776.
3 (*a*) M. A. Shannon, P. W. Bohn, M. Elimelech, J. G. Georgiadis, B. J. Marinas and A. M. Mayes, *Nature*, 2008, **452**, 301–310; (*b*) J. Schaum, M. Cohen, S. Perry, R. Artz, R. Draxler, J. B. Frithsen, D. Heist, M. Lorber and L. Phillips, *Environ. Sci. Technol.*, 2010, **44**, 9383–9389.
4 (*a*) R. Williams, S. Gero, L. Bejder, J. Calambokidis, S. D. Kraus, D. Lusseau, A. J. Read and J. Robbins, *Conserv. Lett.*, 2011, **4**, 228–233; (*b*) I. B. Ivshina, M. S. Kuyukina, A. V. Krivoruchko, A. A. Elkin, S. O. Makarov, C. J. Cunningham, T. A. Peshkur, R. M. Atlas and J. C. Philp, *Environ. Sci.:Processes Impacts*, 2015, **17**, 1201.
5 (*a*) G. Guidi, M. Sliskovic, A. C. Violante and L. Vukic, *Environ. Sci. Pollut. Res.*, 2016, **23**, 1944–1953; (*b*) N. P. Ventikos, E. Vergetis, H. N. Psaraftis and G. Triantafyllou, *J. Hazard. Mater.*, 2004, **107**, 51–58; (*c*) K. Gaaseidnes and J. Turbeville, *Pure Appl. Chem.*, 1999, **71**, 95–101.
6 (*a*) R. K. Gupta, G. J. Dunderdale, M. W. England and A. Hozumi, *J. Mater. Chem. A*, 2017, **5**, 16025–16058; (*b*) G. Kwon, A. K. Kota, Y. Li, A. Sohani, J. M. Mabry and A. Tuteja, *Adv. Mater.*, 2012, **24**, 3666–3671; (*c*) D. S. Etkin and T. J. Nedwed, *Mar. Pollut. Bull.*, 2021, **163**, 111848.
7 (*a*) B. Wang, W. Liang, Z. Guo and W. Liu, *Chem. Soc. Rev.*, 2015, **44**, 336–361; (*b*) S. B. Joye, *Science*, 2015, **349**, 592–593.
8 (*a*) M. O. Adebajo, R. L. Frost, J. T. Kloprogge, O. Carmody and S. Kokot, *J. Porous Mater.*, 2003, **10**, 159–170; (*b*) P. Song, J. Cui, J. Di, D. Liu, M. Xu, B. Tang, Q. Zeng, J. Xiong, C. Wang, Q. He, L. Kang, J. Zhou, R. Duan, B. Chen, S. Guo, F. Liu, J. Shen and Z. Liu, *ACS Nano*, 2020, **14**, 595–602.
9 (*a*) M. M. Radetic, D. M. Jocic, P. M. Jovancic, Z. L. Petrovic and H. F. Thomas, *Environ. Sci. Technol.*, 2003, **37**, 1008–1012; (*b*) A. Malik, S. Sajjad, S. A. K. Leghari, Y. Naz, M. Masood, I. Ahmad and B. Uzair, *Appl. Nanosci.*, 2021, **11**, 1211–1223.
10 (*a*) A. Bayat, S. F. Aghamiri, A. Moheb and G. R. Vakili-Nezhaad, *Chem. Eng. Technol.*, 2005, **28**, 1525–1528; (*b*) J. Ge, H. Y. Zhao, H. W. Zhu, J. Huang, L. A. Shi and S. H. Yu, *Adv. Mater.*, 2016, **28**, 10459–10490.
11 (*a*) L. Huang, Q. Wu, Q. Wang and M. Wolcott, *ACS Sustainable Chem. Eng.*, 2019, **7**, 15920–15927; (*b*) P. Li, Q. Cai, W. Lin, B. Chen and B. Zhang, *Mar. Pollut. Bull.*, 2016, **110**, 6–27.
12 (*a*) Y. Guan, D. Qiao, L. Dong, X. Chen, Z. Wang and Y. Li, *J. Chem. Eng.*, 2023, **467**, 143532; (*b*) M. M. Tijani, A. Aqsha and N. Mahinpey, *J. Environ. Manage.*, 2016, **171**, 166–176.
13 (*a*) Ch. Teas, S. Kalligeros, F. Zanikos, S. Stournas, E. Lois and G. Anastopoulos, *Desalination*, 2001, **140**, 259–264; (*b*) D. Wu, L. Fang, Y. Qin, W. Wu, C. Mao and H. Zhu, *Mar. Pollut. Bull.*, 2014, **84**, 263–267.
14 H. Gao, Y. Liu, G. Wang, S. Li, Z. Han and L. Ren, *Langmuir*, 2019, **35**, 4498–4508.
15 Y. Wei, H. Qi, X. Gong and S. Zhao, *Adv. Mater. Interfaces*, 2018, **5**, 1800576.
16 (*a*) Z. H. Zhang, H. J. Wang, Y. H. Liang, X. J. Li, L. Q. Ren, Z. Q. Cui and C. Luo, *Sci. Rep.*, 2018, **8**, 1–12; (*b*) J. Wang, J. Wu and F. Han, *J. Cleaner Prod*, 2019, **241**, 118369.
17 (*a*) C. Xiao, L. Si, Y. Liu, G. Guan, D. Wu, Z. Wang and X. Hao, *J. Mater. Chem. A*, 2016, **4**, 8080–8090; (*b*) B. Shi, X. Jia and Z. Guo, *New J. Chem.*, 2018, **42**, 17563–17573.
18 (*a*) Q. Zhang, Y. Cao, N. Liu, W. Zhang, Y. Chen, X. Lin, Y. Wei, L. Feng and L. Jiang, *J. Mater. Chem. A*, 2016, **4**, 18128–18133; (*b*) W. Liu, X. Bai, Y. Shen, P. Mu, Y. Yang and J. Li, *Sep. Purif. Technol.*, 2020, **231**, 115899.
19 (*a*) C. Zhou, Z. Chen, H. Yang, K. Hou, X. Zeng, Y. Zheng and J. Cheng, *ACS Appl. Mater. Interfaces*, 2017, **9**, 9184–9194; (*b*) Y. Yang, Z. Guo and W. Liu, *Small*, 2002, **18**, 2204624.
20 (*a*) M. N. Kavalenka, F. Vüllers, F. J. Kumberg, C. Zeiger, V. Trouillet, S. Stein, T. T. Ava, C. Li, M. Worgull and H. Hölscher, *Sci. Rep.*, 2017, **7**, 39970; (*b*) A. Beagan, C. Chen and M. E. Mohamed, *Water Sci. Technol.*, 2024, **89**, 799–810.
21 (*a*) H. Gao, Y. Liu, G. Wang, S. Li, Z. Han and L. Ren, *Langmuir*, 2019, **35**, 4498–4508; (*b*) S. Xu, Q. Wang, N. Wang, X. Zheng and L. Lei, *Colloids Surf., A*, 2019, **583**, 124010.

22 (*a*) X. Gao, J. Zhou, R. Du, Z. Xie, S. Deng, R. Liu, Z. Liu and J. Zhang, *Adv. Mater.*, 2016, **28**, 168–173; (*b*) X. Zheng, Z. Guo, D. Tian, X. Zhang, W. Li and L. Jiang, *ACS Appl. Mater. Interfaces*, 2015, **7**, 4336–4343.
23 (*a*) J. Peng, L. Wu, H. Zhang, B. Wang, Y. Si, S. Jin and H. Zhu, *Chem. Commun.*, 2022, **58**, 11201–11219; (*b*) X. Zhu, Z. Zhang, B. Ge, X. Men, X. Zhou and Q. Xue, *J. Colloid Interface Sci.*, 2014, **432**, 105–108.
24 (*a*) C. Sanchez, P. Belleville, M. Popall and L. Nicole, *Chem. Soc. Rev.*, 2011, **40**, 696–753; (*b*) Y. Si and Z. Guo, *Nanoscale*, 2015, **7**, 5922–5946.
25 (*a*) L. Li, B. Li, J. Dong and J. Zhang, *J. Mater. Chem. A*, 2016, **4**, 13677–13725; (*b*) Y. Hu, C. Huang, D. Su, Q. Jiang and Y. Zhu, *Appl. Surf. Sci.*, 2011, **257**, 6044–6048.
26 (*a*) R. H. Baney, M. Itoh, A. Sakakibara and T. Suzuki, *Chem. Rev.*, 1995, **95**, 1409–1430; (*b*) P. G. Harrison, *J. Organomet. Chem.*, 1997, **542**, 141–183; (*c*) M. G. Voronkov and V. I. Lavrentyev, *Top. Curr. Chem.*, 1982, **102**, 199–236.
27 (*a*) Q. Ye, H. Zhou and J. Xu, *Chem. – Asian J.*, 2016, **11**, 1322–1337; (*b*) Y. Du and H. Liu, *Dalton Trans.*, 2020, **49**, 5396–5405.
28 (*a*) D. B. Cordes, P. D. Lickiss and F. Rataboul, *Chem. Rev.*, 2010, **110**, 2081–2173; (*b*) P. P. Pescarmona and T. Maschmeyer, *Aust. J. Chem.*, 2001, **54**, 583–596; (*c*) R. M. Laine and F. R. Mark, *Macromolecules*, 2011, **44**, 1073–1109.
29 (*a*) S. Shanmugan, D. Cani and P. P. Pescarmona, *Chem. Commun.*, 2014, **50**, 11008–11011; (*b*) M. F. Roll, M. Z. Asuncion, J. Kampf and R. M. Laine, *ACS Nano*, 2008, **2**, 320–326; (*c*) D. Neumann, M. Fisher, L. Tran and J. G. Matisons, *J. Am. Chem. Soc.*, 2002, **124**, 13998–13999.
30 (*a*) E. Carbonell, L. A. Bivona, L. Fusaro and C. Aprile, *Inorg. Chem.*, 2017, **56**, 6393–6403; (*b*) K. Naka, M. Fujita, K. Tanaka and Y. Chujo, *Langmuir*, 2007, **23**, 9057–9063; (*c*) C. Zhang and R. M. Laine, *J. Am. Chem. Soc.*, 2000, **122**, 6979–6988.
31 (*a*) K. Tanaka and Y. Chujo, *J. Mater. Chem.*, 2012, **22**, 1733–1746; (*b*) M. Bahrami, X. Zhang, M. Ehsani, Y. Jahani and R. M. Laine, *Dalton Trans.*, 2017, **46**, 8797–8808; (*c*) Ł. John, M. Janeta and S. Szafert, *New J. Chem.*, 2018, **42**, 39–47.
32 (*a*) H. Liu, S.-I. Kondo, N. Takeda and M. Unno, *J. Am. Chem. Soc.*, 2008, **130**, 10074–10075; (*b*) Y. Leng, J. Zhao, P. Jiang and D. Lu, *Catal. Sci. Technol.*, 2016, **6**, 875–881; (*c*) Z. Wang, S. Leng, Z. Wang, G. Li and H. Yu, *Macromolecules*, 2011, **44**, 566–574; (*d*) A. Santiago-Portillo, V. Cinà, E. Carbonell, L. Fusaro, V. Lemaur, R. Lazzaroni, M. Gruttadauria, F. Giacalone and C. Aprile, *Mater. Adv.*, 2022, **3**, 570–578.
33 (*a*) K. Hou, Y. Zeng, C. Zhou, J. Chen, X. Wen, S. Xu, J. Cheng and P. Pi, *Chem. Eng. J.*, 2018, **332**, 150–159; (*b*) H. Wang, Y. Xue, J. Ding, L. Feng, X. Wang and T. Lin, *Angew. Chem., Int. Ed.*, 2011, **50**, 11433–11436.
34 (*a*) G. Luo, L. Wang, X. Li, K. Yang, Y. Luo, S. Xu and X. Wen, *Soft Matter*, 2019, **15**, 9727–9732; (*b*) Y. Deng, D. Han, Y. Y. Deng, Q. Zhang, F. Chen and Q. Fu, *Chem. Eng. J.*, 2020, **379**, 122391.
35 (*a*) A. Tuteja, W. Choi, M. Ma, J. M. Mabry, S. A. Mazzella, G. C. Rutledge, G. H. McKinley and R. E. Cohen, *Science*, 2007, **318**, 1618–1622; (*b*) A. K. Kota, Y. Li, J. M. Mabry and A. Tuteja, *Adv. Mater.*, 2012, **24**, 5838–5843.
36 S. Pan, A. K. Kota, J. M. Mabry and A. Tuteja, *J. Am. Chem. Soc.*, 2013, **135**, 578–581.
37 A. K. Kota, G. Kwon, W. Choi, J. M. Mabry and A. Tuteja, *Nat. Commun.*, 2012, **3**, 1025.
38 C. Zhang, P. Li and B. Cao, *Ind. Eng. Chem. Res.*, 2015, **54**, 8772–8781.
39 S. Chen, X. Li, Y. Li and J. Sun, *ACS Nano*, 2015, **9**, 4070–4076.
40 E. S. Sanil, K.-H. Cho, D.-Y. Hong, J. S. Lee, S.-K. Lee, S. G. Ryu, H. W. Lee, J.-S. Chang and Y. K. Hwang, *Chem. Commun.*, 2015, **51**, 8418–8420.
41 (*a*) P. Loganathan, K. K. R. Datta and S. Shanmugan, *Inorg. Chem. Front.*, 2021, **8**, 2288–2298; (*b*) K. Dharmaraj, M. S. Kumar, N. Palanisami, M. Prakash, P. Loganathan and S. Shanmugan, *Dalton Trans.*, 2024, **53**, 13602–13616.
42 (*a*) D. R. Dreyer, S. Park, C. W. Bielawski and R. S. Ruoff, *Chem. Soc. Rev.*, 2010, **39**, 228–240; (*b*) T. Torres, *Chem. Soc. Rev.*, 2017, **46**, 4385–4386; (*c*) Q. Xu, H. Xu, J. Chen, Y. Lv, C. Dong and T. S. Sreeprasad, *Inorg. Chem. Front.*, 2015, **2**, 417–424; (*d*) N. F. D. Junaidi, N. H. Othman, N. S. Fuzil, M. S. M. Shayuti, N. H. Alias, M. Z. Shahruddin and N. D. Aba, *Sep. Purif. Technol.*, 2021, **258**, 118000.
43 Y. Xue, Y. Liu, F. Lu, J. Qu, H. Chen and L. Dai, *J. Phys. Chem. Lett.*, 2012, **3**, 1607–1612.
44 Y. Liu, J. Zhou, E. Zhu, J. Tang, X. Liu and W. Tang, *Carbon*, 2015, **82**, 264–272.
45 (*a*) O. Jankovský, V. Mazánek, K. Klímová, D. Sedmidubský, J. Kosina, M. Pumera and Z. Sofer, *Chem. – Eur. J.*, 2016, **22**, 17696–17703; (*b*) F. Karlicky, K. K. R. Datta, M. Otyepka and R. Zboril, *ACS Nano*, 2013, **7**, 6434–6464.
46 (*a*) K. I. Ho, C. H. Huang, J. H. Liao, W. Zhang, L. J. Li, C. S. Lai and C. Y. Su, *Sci. Rep.*, 2014, **4**, 5893; (*b*) X. Chen, K. Fan, Y. Liu, Y. Li, X. Liu, W. Feng and X. Wang, *Adv. Mater.*, 2022, **34**, 2101665.
47 (*a*) K. Jayaramulu, K. Kumara, R. Datta, C. Rçsler, M. Petr, M. Otyepka, R. Zboril and R. A. Fischer, *Angew. Chem., Int. Ed.*, 2016, **55**, 1178–1182; (*b*) K. K. R. Datta, *ChemNanoMat*, 2023, **9**, e202300135.
48 (*a*) R. Yogapriya and K. R. D. Kasibhatta, *ACS Appl. Nano Mater.*, 2020, **3**, 5816–5825; (*b*) I. Prasanthi and K. K. R. Datta, *Inorg. Chem.*, 2023, **62**, 17791–17803.
49 (*a*) Y. Kawakami and Y. Kabe, *Chem. Lett.*, 2010, **39**, 1082–1083; (*b*) L. Liu, Y. Hu, L. Song, X. Gu, Y. Chen and Z. Ni, *Microporous Mesoporous Mater.*, 2010, **132**, 567–571.
50 D. Zhang, R. Yang, Z. Qin and L. Li, *Mater. Lett.*, 2023, **351**, 134982.
51 (*a*) C. Sun, Y. Feng, Y. Li, C. Qin, Q. Zhang and W. Feng, *Nanoscale*, 2014, **6**, 2634–2641; (*b*) L. Liu, Y. Hu, L. Song, X. Gu, Y. Chen and Z. Ni, *Microporous Mesoporous Mater.*, 2010, **132**, 567–571.

52 (*a*) K. Olsson and C. Gronwall, *Ark. Kemi*, 1961, **17**, 529–540; (*b*) K. Song, Y. Jiang and Z. Zou, *ChemistrySelect*, 2020, **5**, 11438–11445.
53 (*a*) X. Ye, L. Ma, Z. Yang, J. Wang, H. Wang and S. Yang, *ACS Appl. Mater. Interfaces*, 2016, **8**, 7483–7488; (*b*) S. Wang, L. Tan, C. Zhang, I. Hussain and B. Tan, *J. Mater. Chem. A*, 2015, **3**, 6542–6548.
54 Y. Liu, Y. Wang, T. C. Zhang, L. Ouyang and S. Yuan, *Sep. Purif. Technol.*, 2024, **331**, 125730.
55 (*a*) E. Ozkan, M. Garren, J. Manuel, M. Douglass, R. Devine, A. Mondal, A. Kumar, M. Ashcraft, R. Pandey and H. Handa, *ACS Appl. Mater. Interfaces*, 2023, **15**, 7610–7626; (*b*) T. Zhang, C. Xiao, J. Zhao, J. Cheng, K. Chen and Y. Huang, *ACS Omega*, 2019, **4**, 7237–7245.